Whispering gallery modes in hexagonal microcavities

Hiroshi Kudo, Ryo Suzuki, and Takasumi Tanabe*
Department of Electronics and Electrical Engineering, Faculty of Science and Technology, Keio University, 3-14-1 Hiyoshi Kohoku-ku, Yokohama 223-8522, Japan
(Received 12 April 2013; published 6 August 2013)

We investigated the whispering gallery modes (WGMs) of cavities with a hexagonal cross section. We found two different modes, namely, perturbed and quasi-WGMs, of which the former exhibits a Q of greater than 10^7 when the corner radii are large and 1.8×10^4 when the corners are sharp. We studied the dependence of Q on the curvature radius of the polygonal cavities and found that the coupling between the two modes determines the Q of the cavity.

DOI: 10.1103/PhysRevA.88.023807 PACS number(s): 42.79.−e, 42.60.Da, 78.20.Bh

I. INTRODUCTION

Optical microcavities such as photonic crystal nanocavities [1,2], microring resonators [3], toroidal microcavities [4], and crystalline whispering gallery mode (WGM) cavities [5] are attractive platforms for studying the optical linear and nonlinear properties of light [6,7]. These cavities have been employed in various studies, including work on slow light generation [1,8,9], an ultranarrow-linewidth laser [10], an optoelectronic oscillator [11,12], nonlinear switching [3,13], frequency-comb generation [6,14], optomechanics [15], frequency conversion [16,17], and nanoparticle sensing [18,19]. WGM cavities, which use internal reflection for light confinement, are particularly attractive because they can provide a very high quality factor Q. Recent progress on the Q factor in such cavities has been noteworthy. In particular, cavities made of SiO_2 such as toroidal [20] and bottle [21] cavities exhibit a very high Q exceeding 10^9 because SiO_2 is a low-loss material and the laser reflow process is well established. On the other hand, WGM cavities made of crystal materials also exhibit an ultrahigh Q, because their absorption loss is even lower than that of SiO_2 [10]. Indeed, Savchenkov *et al.* achieved a Q over 2×10^{10} with a WGM cavity made by CaF_2. Crystalline materials are also attractive because they have various unique properties. The large $\chi^{(2)}$ nonlinearity is essential for making building blocks for optoelectronic modulators [11]. It is transparent at infrared wavelengths, which is an interesting regime for gas sensing [22]. It also has a large Young's modulus, which is attractive for optomechanics research [23]. With the development of ultraprecise machining, the properties of microresonators made of crystal materials have improved, and they are now good candidates, especially as a platform on which to study nonlinear optics.

However, a high-Q crystalline WGM cavity is still difficult to fabricate because the material is hard and frangible. In particular, the fabrication of a small cavity remains a challenge. Previously, we reported on the fabrication of sapphire (Al_2O_3) WGM cavities by employing a modified laser-heated pedestal growth (LHPG) method to overcome this problem [24]. The LHPG method was originally developed for manufacturing fiber lasers [25,26]. It has been applied to various materials such as Al_2O_3, $LiNbO_3$, and YAG [27]. In contrast to earlier work, in which researchers tried to fabricate crystal rods with a thinner and uniform radius, we used this method to fabricate a rod with a locally modulated radius to enable light confinement in the longitudinal direction and excite the WGM. Changing the growth rate enabled us to fabricate a swollen region, in which we obtained a WGM with a Q of 1.6×10^4. In our previous work, we demonstrated the fabrication of sapphire WGM cavities that have a hexagonal cross section but with round edges [24]. The experiment showed that the controllability of the cross section (the sharpness of the edges) is the key to controlling the Q factor of such a cavity. Although this result appears to be straightforward, we need to understand the physics in order to quantitatively design the required structure for having high Q.

In this paper, we analyze in detail various WG-like modes excited in hexagonal cavities with different corner curvatures. In particular, we study a quasi-WGM and a perturbed WGM. By understanding the property of the perturbed-WGM and investigating the coupling between these two modes, we reveal the limit of the Q of the quasi-WGM and study a possible way of improving the value.

The polygonal cavity analysis described in this paper is useful for cavities fabricated with LHPG [24]; moreover it provides information needed to understand the optical properties of a polygonal microlasers made by various materials such as ZnO and InGaAs [28,29]. It is known that these microcavities have a polygonal cross section as a result of their crystal structure, and various experimental and numerical studies have been conducted to understand the mode property of such cavities. Crystals were grown experimentally with different deposition temperatures. Dietrich *et al.* tried to improve the Q value by rounding the corners of polygons [30]. However, the reported Q of these microresonators remains on the order of several thousand, even though the excited modes, which they call a "quasi-WGM," seem to satisfy the total internal reflection in a ray-optics framework [31]. Since we have the same problem in our sapphire hexagonal cavity, the purpose of the first half of this paper is to provide a clear understanding of the limiting Q of this mode in a polygonal cavity.

This paper is organized as follows. In Sec. II we introduce the structure of the cavity we fabricated for investigation. We investigate the properties of the perturbed WGM and quasi-WGM, paying particular attention to the influence of the coupling between these two modes. In Sec. III we describe the relationship between Q and the corner radius of the hexagonal

*takasumi@elec.keio.ac.jp

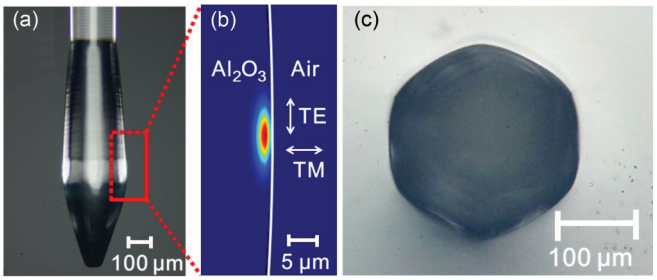

FIG. 1. (Color online) (a) Side view of the fabricated sapphire WGM microcavity. (b) TM-mode profile calculated with the finite-element method (COMSOL MULTIPHYSICS 4.3). (c) Cross section of the fabricated sapphire WGM microcavity.

shape. Then in Sec. IV we explain the optimal radius in order to obtain higher Q. We conclude the paper in Sec. V.

II. ANALYSIS OF THE HEXAGONAL CAVITY

A. Shape of the microcavity fabricated by LHPG

Before analyzing a hexagonal cavity with round corners, we show side and cross-sectional views of our hexagonal sapphire cavity fabricated by LHPG in Fig. 1. We describe the fabrication and optical measurement of this cavity in detail in the Appendix. As shown in Fig. 1(a) the radius of the grown rod is locally modulated. The light is confined in an area where the circumference is the largest, as shown in Fig. 1(b). The typical mode volume is 8.9×10^3 μm^3. Figure 1(c) shows an optical microscope image of the cross section of this cavity. The shape is hexagonal as a result of the crystal structure of the sapphire. However, the corners of the cavity are not sharp but round, and their curvature radius can be controlled by changing the growth condition. This cavity is of interest in mode analysis.

B. Definition of modes

Figure 2 shows the ray-optics description of the possible modes in a hexagonal cavity with slightly rounded corners.

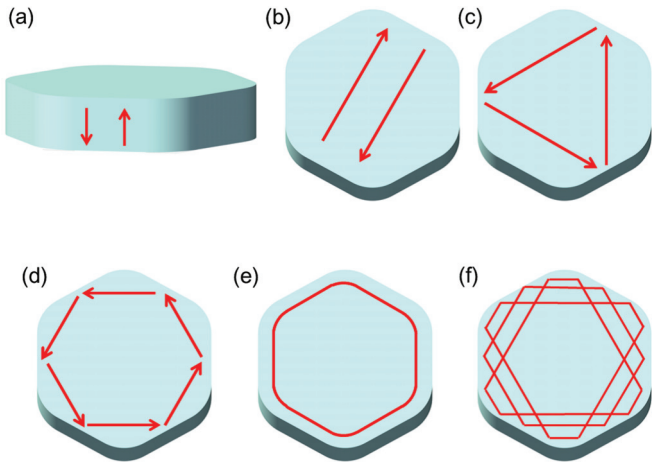

FIG. 2. (Color online) Illustrations of ray-optics descriptions of possible resonant cavity modes in hexagonal geometry. (a) and (b) Fabry-Pérot modes. (c) and (d) Quasi-WGM. (e) Perturbed WGM. (f) Higher-order quasi-WGM.

Fabry-Pérot (FP) modes [Figs. 2(a) and 2(b)] are excited by reflection at the opposing disk facets or at the hexagonal facets. Figures 2(c) and 2(d) show "quasi-WGMs" in which light is reflected at the side of the polygon. Since these modes satisfy the total internal reflection in a ray-optics framework, the quasi-WGM appears to exhibit an ultrahigh Q. Although the quasi-WGM has been studied in detail in previous work [31], we will show below that the discovery of a different WGM, which is shown in Fig. 2(e), is essential if we are to understand the low Q of the quasi-WGM. We call this mode a "perturbed WGM" [32] because this is an ultrahigh-Q WGM when the cavity is round. A complete understanding of these modes is the main aim of this paper. In addition, we show that a different mode, shown in Fig. 2(f), which has usually been categorized as a quasi-WGM, originates from a higher-order WGM.

To investigate these modes in detail we perform a two-dimensional finite-difference time-domain (FDTD) calculation. Figure 3(a) shows the structure that we used for the calculation. It is a hexagonal cavity with round corners that have curvature radii r.

When the microcavity is a perfect circle, an ideal WGM is excited, as shown in Fig. 3(b). Next, we change r and make the cavity slightly polygonal. Then we obtain an optical mode, as shown in Fig. 3(c). This is the quasi-WGM shown in Fig. 2(d). The light propagates while being reflected at the side of the cavity. This simple picture leads us to expect that the resonant wavelength and the Q of the quasi-WGM do not depend strongly on the edge radius r.

In contrast, we obtained a different mode in a hexagonal cavity for the same geometry as shown in Fig. 3(d). This is the perturbed WGM. The original circular WGM is perturbed

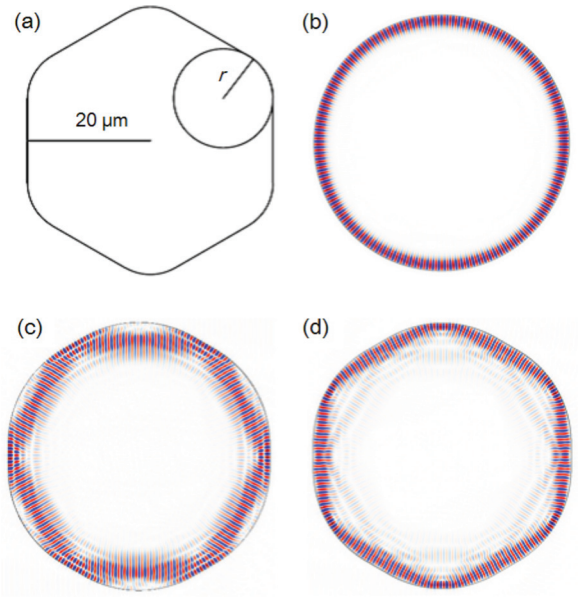

FIG. 3. (Color online) (a) Model used for FDTD calculations. The refractive index of the cavity is 1.74. The cavity radius is 20 μm, and the edge radius is r. (b) Mode profile of a WGM when the shape is a perfect circle ($r = 20$ μm). (c) Mode profile of a quasi-WGM when $r = 16.1$ μm. (d) Mode profile of a perturbed WGM when $r = 16.1$ μm.

as a result of the modulation of the structure from circular to hexagonal. But it retains the WGM characteristics, where the light propagates close to the surface. Note that if we look very carefully, we find that the light of this mode propagates close to the surface at the corner, but it propagates slightly inwards at the side [32]. In contrast to the quasi-WGM, with the perturbed WGM we can straightforwardly predict that the resonant wavelength and Q value change sensitively according to the corner radius r.

Since this mode exhibits an ultrahigh Q when the corner is round, we expect the Q of the perturbed WGM to be higher than that of the quasi-WGM when r is large. However, the r dependence of Q is larger for the perturbed WGM; therefore, Q of the quasi-WGM should become higher when the corner is sharp and the cavity is hexagonal. But this simple description is insufficient, as we discuss in the following sections.

III. MODE ANALYSIS

A. Resonant modes in a hexagonal cavity

Figure 4(a) shows the resonance wavelength of the perturbed and quasi-WGMs with respect to the r calculated using the FDTD method. As expected, the resonant wavelength changes much more sensitively in relation to r for the perturbed WGM than for the quasi-WGM. Most importantly, we know from Fig. 4(a) that the WGM of the circular cavity shown in Fig. 3(b) is on the same slope as the perturbed WGM in Fig. 3(d). This indicates that the mode shown in Fig. 3(d) is indeed a perturbed WGM, and the quasi-WGM originates from a different mode from an ultrahigh-Q WGM when the cavity is circular.

Next, we investigate the resonance in more detail. Figure 4(b) shows the resonant spectrum when $r = 17.8\ \mu$m. This spectrum shows that not only two modes but also various other different modes are excited in this hexagonal cavity. To explain the property of the hexagonal cavity, we need to understand these modes. Since it is difficult to characterize the property of this number of modes from this single spectrum, we need to perform calculations with different r.

The resonant peaks for cavities with different r values are shown in Fig. 5(a). The plots for the quasi- and perturbed WGMs shown in Figs. 3(c) and 3(d) are indicated. However, a number of different peaks appear in addition to these two modes. Although the behavior of these modes appears very complicated, they can be classified into two different groups. We clearly obtained two different slopes.

Figure 5(b) shows a quasi-WGM but with a different longitudinal mode number. Similar resonance also appears at an 11.6-nm-longer wavelength, where the interval is the free spectral range (FSR) of this mode. Indeed, we obtained a similar FSR value from a simple ray-optics estimation. Similarly, Fig. 5(c) shows a perturbed WGM with a different longitudinal mode number. The FSR for the perturbed WGM is 11.3 nm.

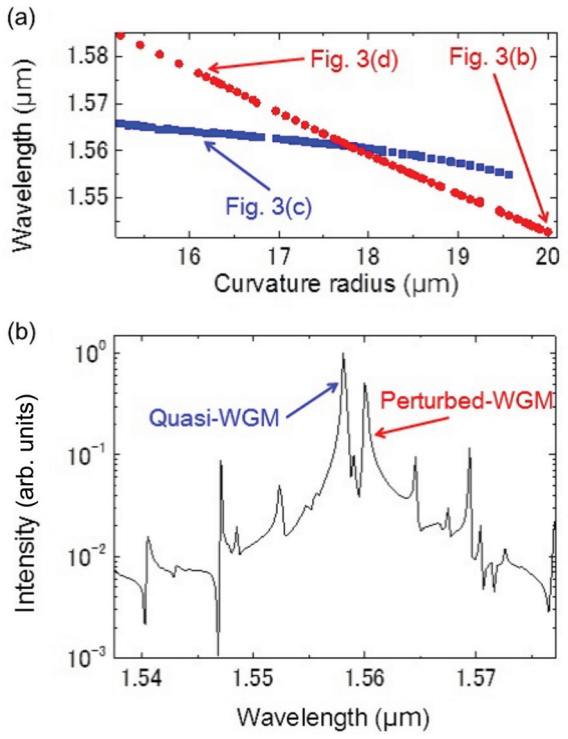

FIG. 4. (Color online) (a) Resonance wavelength of the perturbed WGM and quasi-WGM in relation to the curvature radius r. (b) Spectrum of the excited modes of a hexagonal cavity when $r = 17.8\ \mu$m.

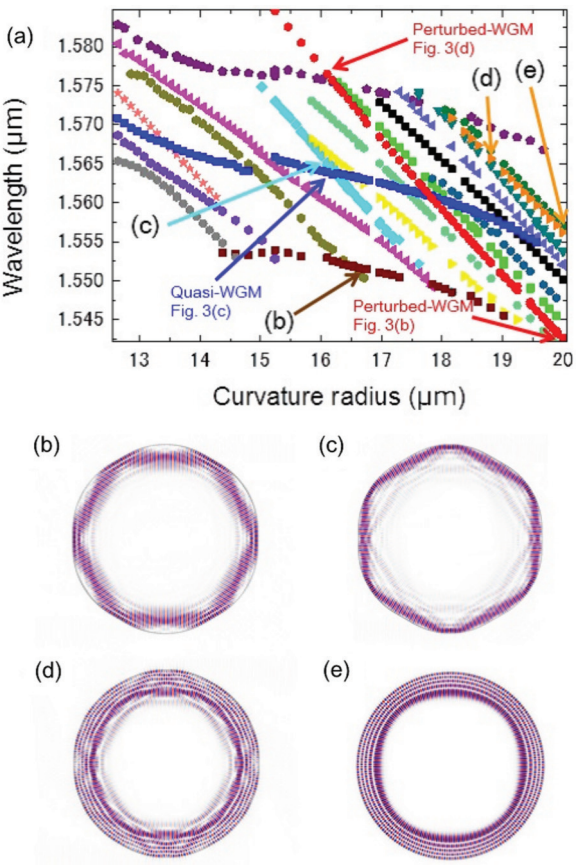

FIG. 5. (Color online) (a) Resonant modes of hexagonal cavities with different curvature radii r. (b)–(e) Mode profiles of the cavity. The corresponding resonance points are shown in (a).

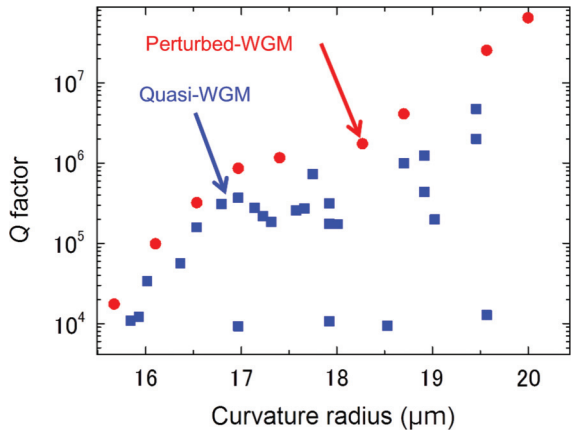

FIG. 6. (Color online) Q of perturbed and quasi-WGMs for a hexagonal cavity with different curvature radius r values.

However, Fig. 5(c) shows that there are a number of different modes with a similar r dependence to that of the perturbed WGM in the hexagonal cavity. One of the modes is shown in Fig. 5(d). In this mode, the light propagates not only at the surface of the cavity but also at the inner part of the structure. This propagation occurs because the light reflects at the cavity wall with a large incident angle. The light propagation in this mode is described in terms of ray optics in Fig. 2(f), where the mode was originally classified as a quasi-WGM. However, the r dependence of this mode in Fig. 5(b) suggests that its behavior is similar to that of the perturbed WGM. Indeed, when we examine the profile at $r = 20\ \mu$m for this mode, namely, when the cavity is circular, we observe a higher-order WGM, as shown in Fig. 5(e). Hence, we can conclude that the mode shown in Fig. 5(d) is the perturbed mode of the higher-order WGM.

It is important to understand this picture because it indicates the difficulty of obtaining an ultrahigh Q for the mode shown in Fig. 5(e), even though the ray-optics image in Fig. 2(f) gives the impression that this mode may exhibit a high Q even when the corner is sharp.

B. Cavity Q of perturbed and quasi-WGMs

Since the quasi- and perturbed WGMs [Figs. 3(c) and 3(d)] are the fundamental modes of this hexagonal cavity, we now focus on these two modes and analyze Q. Figure 6 shows Q for these two modes with different r values. Contrary to our initial expectation, the quasi-WGM exhibits a lower Q when the cavity is polygonal, although Fig. 2(d) suggests that Q is only slightly dependent on r.

To understand this behavior, we pay close attention to the wavelength crossing between the quasi-WGM and the perturbed WGM.

C. Coupling between modes

Figures 7(a) and 7(b) show enhanced views of the crossing points between the perturbed and quasi-WGMs in Fig. 5(a). These figures show that these two modes exhibit anticrossing behavior, which indicates the existence of strong mode coupling between those two modes. We can derive the coupling coefficient κ from the spectrum splitting width, and we

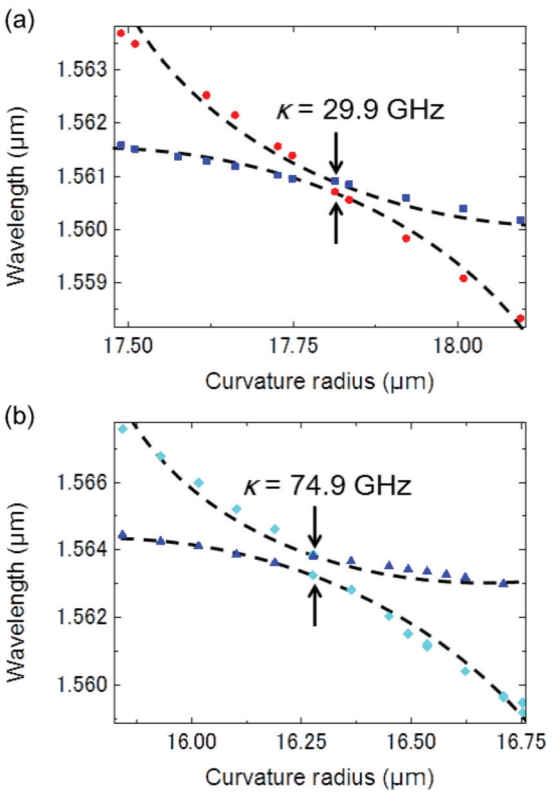

FIG. 7. (Color online) Wavelength crossing between perturbed and quasi-WGMs.

obtained $\kappa = 2.99 \times 10^{10}\ \mathrm{s}^{-1}$ for Fig. 7(a) and $\kappa = 7.49 \times 10^{10}\ \mathrm{s}^{-1}$ for Fig. 7(b). This explains the low-Q property of the quasi-WGM when the corners are sharp.

According to the ray-optics description shown in Fig. 2(d), Q of the quasi-WGM does not depend on the edge radius r of the hexagonal cavity and should exhibit an ultrahigh Q. However, the coupling between the quasi- and perturbed WGMs needs to be taken into account. This coupling is particularly important when r is small. Coupling between modes, for example, $\kappa = 2.99 \times 10^{10}\ \mathrm{s}^{-1}$, which corresponds to a Q of about 3×10^3, means that the light energy of the high-Q perturbed WGM transfers to a low-Q quasi-WGM and then easily couples to the out-of-cavity radiation. Therefore, Q of the quasi-WGM is not dependent on Q of the perturbed WGM, and the values of those two modes become very close. Since the Q value of the perturbed WGM is low when the corner is sharp, the Q value of the quasi-WGM also decreases. The very low Q plots ($\sim 10^4$) of the quasi-WGM in Fig. 6 result from coupling with higher-order perturbed WGMs that have a low Q.

A numerical analysis revealed that Q of quasi-WGM is fundamentally dependent on Q of the perturbed WGM. Since Q of the perturbed WGM is low when the corner radius r is small, it is not easy to obtain an ultrahigh-Q cavity even when we excite the quasi-WGM. Therefore, the only method with the potential to provide an ultrahigh Q in such a crystalline cavity is to make the shape as circular as possible. In the Appendix, we show methods for fabricating circular sapphire WGM cavities by using LHPG to achieve a high Q.

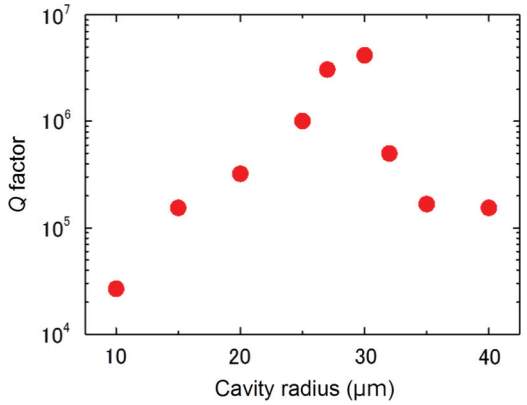

FIG. 8. (Color online) Q factor of a perturbed WGM as a function of the radius R of hexagonal cavities with a curvature radius $r = 0.8R$.

IV. OPTIMAL SIZE OF POLYGONAL CAVITY

In this section, we discuss the optimal radius of the hexagonal cavity. We focus on the perturbed WGM in a hexagonal cavity with a radius R and a curvature radius $r = 0.8R$. It is known that Q of a circular WGM cavity increases linearly as the radius increases [5]. However, this characteristic has not been studied for a polygonal WGM cavity.

Figure 8(a) shows the Q factor for the perturbed WGM for hexagonal cavities with different cavity radii r. It clearly shows that there is an optimal point at $r = 30\ \mu$m. The Q value decreases when d is small because it is difficult for the light in the cavity to satisfy the total internal reflection condition when the cavity is small. Moreover, unlike a circular cavity, the Q value decreases when $r > 30\ \mu$m, which is difficult to explain solely in terms of total internal reflection. A careful investigation revealed that mode coupling plays an important role. In a large cavity, the mode spacing of the lowest-order perturbed WGM and that of the higher-order perturbed WGM are both very small, which results in an easy overlap between these modes. Since higher-order WGMs have a much lower Q, the Q of the lowest-order perturbed WGM also decreases for a large cavity. Therefore, there is an optimum radius in regard to obtaining a higher Q in a hexagonal cavity.

V. CONCLUSION

We investigated excited modes in polygonal cavities in detail and found that a perturbed WGM exhibits an ultrahigh Q when the corner radius of the cavity is large. We found that a number of lower- and higher-order perturbed WGMs are present in a hexagonal cavity coupled with a quasi-WGM. Although the quasi-WGM appears to exhibit an ultrahigh Q with ray optics, mode coupling with the perturbed WGM limits Q of this mode. We revealed that we need to understand the coupling between the modes to explain the low Q of the quasi-WGM when the cavity is hexagonal. As a result, the only way to improve Q of the crystalline cavity (with both sapphire and ZnO cavities) is to make the corner round.

Research using WGM cavities is active in various fields, including microlaser fabrication, quantum optics, sensing, and signal processing. However, the fabrication of a crystalline WGM remains difficult because of its fragility. In our previous study [24], we showed a method to fabricate WGM cavities with modified LHPG. This numerical study will help us understand the characteristics of the cavity modes fabricated with this method as well as with other crystal growth techniques [28,29]. Crystal growth technologies are promising for fabricating small crystalline WGMs, and they may be used for various applications when we clarify the methods and the boundary conditions on having high Q in such cavities.

ACKNOWLEDGMENTS

Part of this work was supported by the Strategic Information and Communications R&D Promotion Programme (SCOPE), a Grant-in-Aid for Scientific Research from the Ministry of Education, Culture, Sports, Science and Technology, Japan (Grant No. KAKEN 25600118), and the Keio University Next Generation Research Project Promotion Program. The authors also thank Dr. Atsushi Yokoo from NTT Basic Research Laboratories and Professor Yasuhiro Kakinuma from Keio University for valuable discussions on LHPG and precise machining, respectively.

APPENDIX: EXPERIMENT

1. Experimental setup

Figure 9 shows the experimental setup for the LHPG method. The input CO_2 laser beam (Coherent DIAMOND C-70) is formed into a doughnut shape by using a pair of axicon lenses. This minimizes the beam that hits the feed rod before it is focused with a concave mirror, and it makes the beam focusing more efficient. The CO_2 laser beam is focused on the feed rod by using a concave mirror with a radius of 50 mm to heat the rod and form a molten zone. The laser beam spot size is about 12.2 μm, and the power density is 8.58×10^7 W/m^2 when the CO_2 laser power is 4.0 W. Both the seed and feed rods are fixed to a linear translation stage (Oriental Motor ASM46MA). The radius of the sapphire single-crystal rods is 213 μm for both the feed and seed rods.

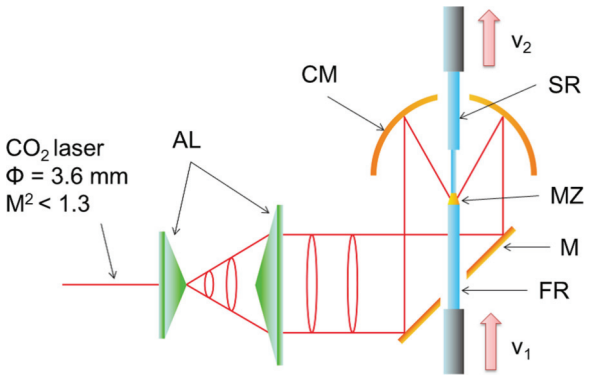

FIG. 9. (Color online) Schematic illustration of experimental setup. AL: ZnSe axicon lens, FR: feed rod, SR: seed rod, M: flat gold mirror with a hole at the center, CM: concave gold mirror (curvature = 100 mm) with a hole at the center, MZ: molten zone. A CO_2 laser with diameter ϕ and beam parameter product M^2 is used to heat the crystal rods.

Then a crystal fiber is grown by pulling the feed rod upwards at a speed of v_1, while the seed rod is moved in the same direction with a speed of v_2 ($v_2 > v_1$). In LHPG, we can control the radius of the grown crystal rods by changing the velocity rate, whose relationship is given by

$$R_1 = R_2 \left(\frac{v_2}{v_1}\right)^{\frac{1}{2}}, \tag{A1}$$

where R_1 and R_2 are the radii of the grown and feed rods, respectively. LHPG was originally developed to create crystal rods with a uniform radius. In contrast, by changing the velocity rate we can create a bulge with which we can confine light in the longitudinal direction and excite the WGM.

In the experiment, we changed the velocity rate from 1/6 to 1/3. This corresponds to calculated R_1 values of 87 and 123 μm when the feed rod radius R_2 is 213 μm. First, we started with standard LHPG. v_1 was set to 2 μm/s, and v_2 was set to 12 μm/s. In brief, v_1/v_2 was 1/6, and the grown rod was fabricated with a radius of 87 μm. Next, we reduced v_2 from 12 to 6 μm/s and set the v_1/v_2 ratio to 1/3 to fabricate a WGM cavity. The grown radius of the WGM cavity was then larger at 123 μm. Finally, we stopped the seed rod and pulled the feed rod downward.

A side view and cross section of the fabricated cavity are shown in Figs. 1(a) and 1(c). The cross section of this cavity is hexagonal as a result of the crystalline structure of the sapphire. As discussed earlier, it is essential to develop a method for controlling the curvature of the edge radius of this cavity in order to increase Q. We already showed the basic idea of the preheating method in our previous work [24]. Here, we show in more detail the controllability of the fabrication.

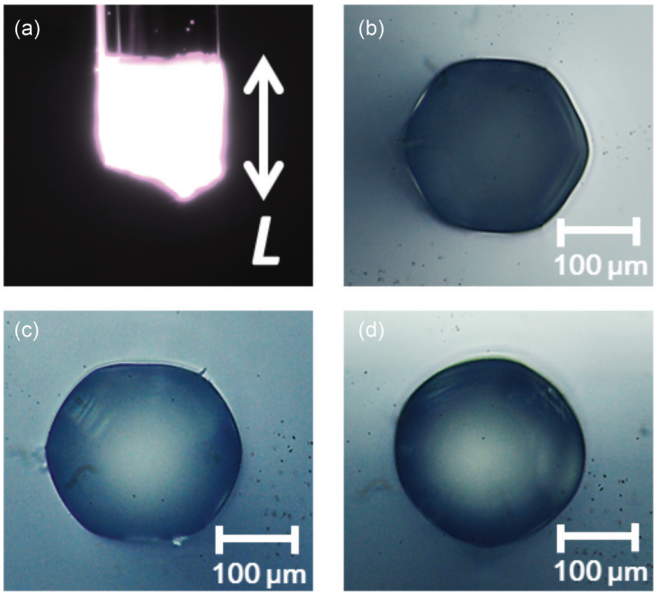

FIG. 10. (Color online) (a) Optical microscope image of a seed rod during the preheating process. L is the length of the preheated region. Optical microscope image of a cross section of the fabricated sapphire cavity with different L values: (b) $L = 0.10$ mm, (c) $L = 0.70$ mm, and (d) $L = 0.78$ mm.

2. Control of cross-section geometry

We introduce a preheating method to make the cavity round. The seed rod is heated with a CO_2 laser at a power of 8 W prior to the crystal growth. Figure 10(a) shows the 213-μm-radius preheating seed rod, where L is the heating length. We changed L and observed the cross-sectional shape of the fabricated WGM cavity. Figures 10(b)–10(e) show the cross section of the fabricated sapphire cavity with different L values. When L is larger, the cross-sectional shape becomes close to a circle.

This experimental result clearly shows that the preheating method is a promising way to change the cross-sectional shape of the cavity. However, we observed that the cross section often deforms when L is 0.80 mm or larger. The cross section of the cavity changes because we change the growth axis by introducing preheating to the seed rod. Indeed, x-ray diffraction of the fabricated crystals show peaks of high-order crystal planes, which is an indication of the tilt of the c axis.

3. Optical measurement

We measured the transmittance spectrum of the sapphire microcavity in Fig. 11(a) by coupling light with an optical

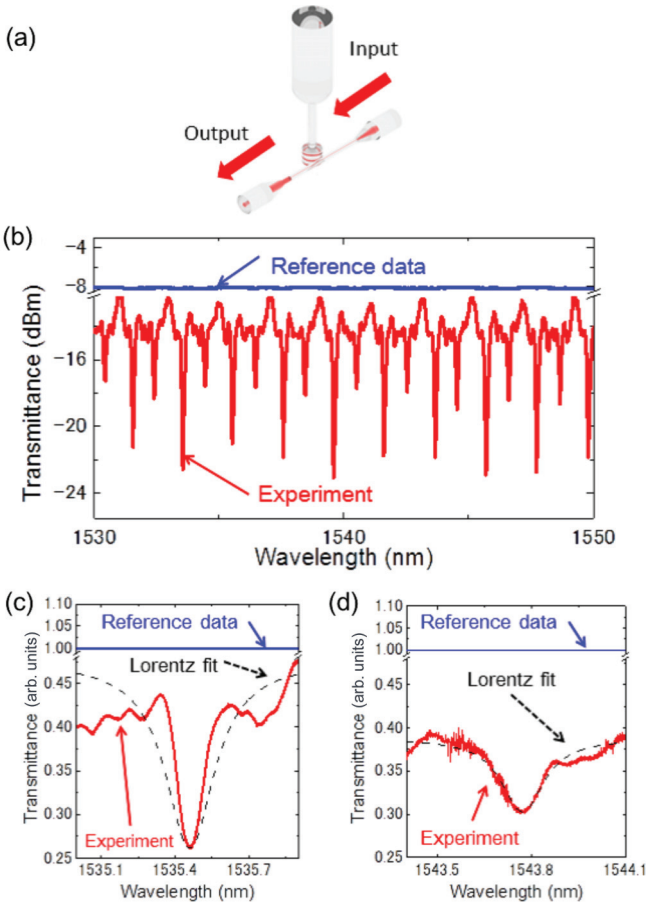

FIG. 11. (Color online) (a) Schematic illustration of optical experimental setup using a conventional tapered fiber. (b) Transmission spectrum of a circular cavity fabricated using preheating. (c) Enlarged image of (b). The dashed line is a Lorentzian fit for the experimental data, whose width gives a Q of 1.6×10^4. (d) Transmission spectrum of the hexagonal cavity without preheating. It has a Q of 8.5×10^3.

tapered fiber setup. We can control the coupling between the resonator and the waveguide in order to measure the cavity Q. The transmittance spectrum of a circular sapphire WGM cavity is shown in Fig. 11(b). We observe clear resonance with an equal free spectral range. Figure 11(c) is an enlarged view of Fig. 11(b). By fitting the spectrum with a Lorentzian shape, we obtained a Q of 1.6×10^4. This value is higher than that obtained from the resonant spectrum of a hexagonal cavity shown in Fig. 11(d), which has a Q of 8.5×10^3. As expected, with a numerical analysis, we obtained a higher Q for a circular cavity than for a hexagonal cavity.

Although theory and experiment both predict a higher Q for a circular cavity and are in a good agreement, the absolute Q values are far apart. The surface roughness of the cavity was 65 nm rms when we grew the crystal at a speed of 12 μm/s. Following Ref. [5], Q is inversely proportional to the square of the surface roughness. When we substitute the experimental values, we obtained a Q of about 10^4. Therefore, we conclude that the experimental Q is now limited by the surface roughness. Our preliminary experiments show that the surface roughness can be reduced to 6 nm rms by reducing the crystal growth speed to 2 μm/s.

[1] T. Tanabe, M. Notomi, E. Kuramochi, A. Shinya, and H. Taniyama, Nat. Photonics **1**, 49 (2007).

[2] Y. Akahane, T. Asano, B. S. Song, and S. Noda, Nature (London) **425**, 944 (2003).

[3] V. R. Almeida, C. A. Barrios, R. R. Panepucci, and M. Lipson, Nature (London) **431**, 1081 (2004).

[4] P. Del'Haye, A. Schliesser, O. Arcizet, T. Wilken, R. Holzwarth, and T. J. Kippenberg, Nature (London) **450**, 1214 (2007).

[5] I. S. Grudinin, A. B. Matsko, A. A. Savchenkov, D. Strekalov, V. S. Ilchenko, and L. Maleki, Opt. Commun. **265**, 33 (2006).

[6] T. J. Kippenberg, R. Holzwarth, and S. A. Diddams, Science **332**, 555 (2011).

[7] W. Yoshiki and T. Tanabe, J. Opt. Soc. Am. B **29**, 3335 (2012).

[8] M. Notomi, E. Kuramochi, and T. Tanabe, Nat. Photonics **2**, 741 (2008).

[9] Y. A. Vlasov, M. O'Boyle, H. F. Hamann, and S. J. McNab, Nature (London) **438**, 65 (2005).

[10] A. A. Savchenkov, V. S. Ilchenko, A. B. Matsko, and L. Maleki, Phys. Rev. A **70**, 051804(R) (2004).

[11] L. Maleki, Nat. Photonics **5**, 728 (2011).

[12] T. Tanabe, K. Nishiguchi, E. Kuramochi, and M. Notomi, Opt. Express **17**, 22505 (2009).

[13] T. Tanabe, M. Notomi, S. Mitsugi, A. Shinya, and E. Kuramochi, Opt. Lett. **30**, 2575 (2005).

[14] A. A. Savchenkov, A. B. Matsko, V. S. Ilchenko, I. Solomatine, D. Seidel, and L. Maleki, Phys. Rev. Lett. **101**, 093902 (2008).

[15] S. Weis, R. Rivière, S. Deléglise, E. Gavartin, O. Arcizet, A. Schliesser, and T. J. Kippenberg, Science **330**, 1520 (2010).

[16] S.-i. Inoue and Y. Aoyagi, Phys. Rev. Lett. **94**, 103904 (2005).

[17] T. Tanabe, M. Notomi, H. Taniyama, and E. Kuramochi, Phys. Rev. Lett. **102**, 043907 (2009).

[18] T. Lu, H. Lee, T. Chen, S. Herchak, J.-H. Kim, S. E. Fraser, R. C. Flagan, and K. Vahala, Proc. Natl. Acad. Sci. USA **108**, 5976 (2011).

[19] F. Vollmer, S. Arnold, and D. Keng, Proc. Natl. Acad. Sci. USA **105**, 20701 (2008).

[20] D. K. Armani, T. J. Kippenberg, S. M. Spillane, and K. J. Vahala, Nature (London) **421**, 925 (2003).

[21] M. Pöllinger and A. Rauschenbeutel, Opt. Express **18**, 17764 (2010).

[22] C. Y. Wang, T. Herr, P. Del'Haye, A. Schliesser, J. Hofer, R. Holzwarth, T. W. Hänsch, N. Picqué, and T. J. Kippenberg, Nat. Commun. **4**, 1345 (2013).

[23] J. Hofer, A. Schliesser, and T. J. Kippenberg, Phys. Rev. A **82**, 031804(R) (2010).

[24] H. Kudo, Y. Ogawa, T. Kato, A. Yokoo, and T. Tanabe, Appl. Phys. Lett. **102**, 211105 (2013).

[25] A. Yokoo, S. Tomaru, I. Yokohama, H. Itoh, and T. Kaino, J. Cryst. Growth **156**, 279 (1995).

[26] M. M. Fejer, L. J. Nightingale, G. A. Magel, and R. L. Byer, Rev. Sci. Instrum. **55**, 1791 (1984).

[27] R. Feigelson, Mater. Sci. Eng. B **1**, 67 (1988).

[28] T. Nobis, E. M. Kaidashev, A. Rahm, M. Lorenz, and M. Grundmann, Phys. Rev. Lett. **93**, 103903 (2004).

[29] R. Chen, T.-T. D. Tran, K. W. Ng, W. S. Ko, L. C. Chuang, F. G. Sedgwick, and C. C. Hasnain, Nat. Photonics **5**, 170 (2011).

[30] C. P. Dietrich, M. Lange, T. Böntgen, and M. Grudmann, Appl. Phys. Lett. **101**, 141116 (2012).

[31] C. Czekall, T. Nobis, A. Rahm, B. Cao, J. Zúñiga-Peréz, C. Sturm, R. Schmidt-Grund, M. Lorenz, and M. Grundmann, Phys. Status Solidi B **247**, 1282 (2010).

[32] T. Kato, W. Yoshiki, R. Suzuki, and T. Tanabe, Appl. Phys. Lett. **101**, 121101 (2012).